

The Slab Method to Measure the Topological Susceptibility*

Wolfgang Bietenholz^{†a}, Krzysztof Cichy^{b,c}, Philippe de Forcrand^{d,e},
Arthur Dromard^{b,f} and Urs Gerber^{a,g}

^a *Instituto de Ciencias Nucleares, Universidad Nacional Autónoma de México
A.P. 70-543, C.P. 04510 Ciudad de México, Mexico*

^b *Goethe-Universität Frankfurt am Main, Institut für Theoretische Physik
Max-von-Laue-Straße 1, D-60438 Frankfurt am Main, Germany*

^c *Faculty of Physics, Adam Mickiewicz University, Umultowska 85, 61-614 Poznan, Poland*

^d *Institut für Theoretische Physik, ETH Zürich, CH-8093 Zürich, Switzerland*

^e *CERN, Theory Division, CH-1211 Geneva 23, Switzerland*

^f *Institut für Theoretische Physik, Universität Regensburg, D-93040 Regensburg, Germany*

^g *Instituto de Física y Matemáticas, Universidad Michoacana de San Nicolás de Hidalgo
Edificio C-3, Apdo. Postal 2-82, C.P. 58040, Morelia, Michoacán, Mexico*

E-mail: wolbi@nucleares.unam.mx

In simulations of a model with topological sectors, algorithms which proceed in small update steps tend to get stuck in one sector, especially on fine lattices. This distorts the numerical results; in particular it is not straightforward to measure the topological susceptibility χ_t . We test a method to measure χ_t even if configurations from only one sector are available. It is based on the topological charges in sub-volumes, which we denote as “slabs”. This enables the evaluation of χ_t , as we demonstrate with numerical results for non-linear σ -models and for 2-flavour QCD. In the latter case, the gradient flow is applied for the smoothing of the gauge configurations, and the slab method results for χ_t are stable over a broad range of flow times.

*34th International Symposium on Lattice Field Theory
24-30 July 2016
University of Southampton, UK*

*We thank Stephan Dürr, Massimo D’Elia and Marc Wagner for helpful discussions. This work was supported by the Mexican *Consejo Nacional de Ciencia y Tecnología* (CONACYT) through projects CB-2010/155905 and CB-2013/222812, by DGAPA-UNAM, grant IN107915, and by the *Helmholtz International Center for FAIR* within the framework of the LOEWE program launched by the State of Hesse. A.D. acknowledges support by the Emmy Noether Programme of the DFG (German Research Foundation), grant WA 3000/1-1. The computations were performed on the cluster of ICN/UNAM, and on the LOEWE-CSC and FUCHS-CSC high-performance computer of Frankfurt University.

[†]Speaker.

1. The topological susceptibility χ_t

In models with topological sectors, a quantity of interest is the topological susceptibility

$$\chi_t = \frac{1}{V} (\langle Q^2 \rangle - \langle Q \rangle^2), \quad Q : \text{topological charge}, \quad V : \text{volume}. \quad (1.1)$$

We are going to address settings with parity invariance, where χ_t simplifies due to $\langle Q \rangle = 0$.

A prominent application is the Witten-Veneziano formula, as a quantitative solution to the U(1) problem: for three massless quark flavours and large N_c , the $1/N_c$ corrections yield $\chi_t^{\text{quenched}} \simeq F_\pi^2 M_{\eta'}^2 / 6$, where $F_\pi^2 \propto N_c$, and $M_{\eta'}^2 \propto 1/N_c$. For QCD with dynamical quarks, there is a similar relation to a putative axion mass and decay constant, $\chi_t \simeq F_{\text{axion}}^2 M_{\text{axion}}^2$. Hence the value of χ_t (at finite temperature) is relevant for the question whether or not the axion is a valid Cold Dark Matter candidate; for a review and recent lattice results, see *e.g.* Refs. [1].

χ_t can only be determined non-perturbatively, hence numerical measurements in lattice simulations are appropriate. If a Monte Carlo history changes the topological sector frequently, it is straightforward to measure $\langle Q^2 \rangle$ (once one has defined the topological charge of the lattice configurations). This is the case for instance in quenched QCD, simulated with the heatbath algorithm at lattice spacing $a > 0.1$ fm; an example is described in Ref. [2].

Another direct approach is to measure (in lattice units) $\chi_t = \sum_{x \in V} \langle q_0 q_x \rangle$, where q_x is the topological charge density. This has been applied successfully to $2+1$ flavour QCD [3]. The long-distance correlation function was fitted to an expected linear combination of modified Bessel functions K_1 , where the phenomenological values of M_η and $M_{\eta'}$ were inserted.

As we decrease a , however, the topological sectors are separated by higher and higher potential barriers. Then an algorithm which performs small update steps tends to get stuck in one topological sector for a very long (computation) time. According to Ref. [4], the autocorrelation time with respect to Q , τ_Q , in simulations of SU(N) Yang-Mills theories (with the Wilson lattice action, and alternating overrelaxation and heatbath steps), is compatible with an exponential growth, or a high power, in $1/a$. For QCD, Ref. [5] observed a behaviour $\propto (1/a)^z$ with $z \simeq 5$ in the quenched case, and similar with dynamical quarks, represented by $O(a)$ -improved Wilson fermions (though z is less accurate). Dynamical chiral quarks make the growth of τ_Q even worse.

One way to deal with this issue is to modify the algorithm such that changes of Q become more frequent; such efforts are reviewed in Ref. [6]. A different approach suggests the use of open boundary conditions in Euclidean time [7], which removes the topological sectors, $Q \in \mathbb{R}$, but it breaks lattice translation invariance. Here we address yet another concept, which aims at determining χ_t even from data in one fixed (“frozen”) topological sector.

One approach which — in principle — could be used for this purpose is an approximation for some expectation value $\langle \mathcal{O} \rangle$, if only measurements in fixed sectors, $\langle \mathcal{O} \rangle|_Q$, are available [8],

$$\langle \mathcal{O} \rangle|_Q \simeq \langle \mathcal{O} \rangle + \frac{\text{const.}}{V \chi_t} \left(1 - \frac{Q^2}{V \chi_t} \right). \quad (1.2)$$

This is the beginning of an expansion in $1/(V \chi_t) = 1/\langle Q^2 \rangle$, extensions are discussed in Refs. [9, 10]. Once we have a set of results for $\langle \mathcal{O} \rangle|_Q$, in different V and $|Q|$, a fit provides values for the unknown (intensive) quantities: $\langle \mathcal{O} \rangle$, χ_t and the const. A detailed numerical study [10], in a variety of models, shows that this works quite well for the determination of $\langle \mathcal{O} \rangle$ if suitable conditions are fulfilled¹, but the results for χ_t are plagued by large uncertainties.

¹Typically $\langle Q^2 \rangle > 1$ is required, and one should only involve sectors with small $|Q|$.

More successful for the determination of χ_t — though exclusively devoted to that purpose — is an approximation derived in Ref. [11] (in a way similar to Ref. [8]),

$$\langle q_0 q_x \rangle |_{|Q|, \text{large } |x|} \simeq -\frac{\chi_t}{V} \left(1 - \frac{Q^2}{V\chi_t} \right). \quad (1.3)$$

One measures the left-hand side and searches for a plateau of the correlation function over long distances. This determines χ_t , under conditions similar to footnote 1. The problem is to resolve tiny plateau values as the volume increases, but their suppression can be compensated by computing all-to-all correlations [12].

Here we discuss yet another, particularly simple approach, which we denote as the “slab method”.

2. The slab method

The idea of the slab method was first mentioned in Ref. [13] and recently tested in the framework of σ -models [14] and in two flavour QCD [15]. There is some similarity with the method of Ref. [16], and with an instanton-liquid consideration in Ref. [17].

We assume a Gaussian distribution of the topological charge, $p(Q) \propto e^{-Q^2/(2\chi_t V)}$, which is approximately confirmed, see below. Next we split the volume V into sub-volumes of sizes xV and $(1-x)V$ ($0 < x < 1$) — which we denote as *slabs* — as illustrated in Fig. 1. For a configuration with total topological charge Q , the slabs carry charges q and $Q-q$ (obtained by summing up the density). Note that q and $Q-q$ do not need to be integers, because the face between the slabs is a non-periodic boundary. At fixed V, x and Q , the probabilities p_1, p_2 for the slab charges obey

$$p_1(q) \cdot p_2(Q-q) \propto \exp\left(-\frac{q^2}{2\chi_t V x}\right) \cdot \exp\left(-\frac{(Q-q)^2}{2\chi_t V (1-x)}\right) \propto \exp\left(-\frac{1}{2\chi_t V} \frac{q'^2}{x(1-x)}\right), \quad (2.1)$$

where $q' := q - xQ$, and from $\langle q \rangle = xQ$ we infer $\langle q'^2 \rangle = \langle q^2 \rangle - x^2 Q^2$. The idea is to measure $\langle q^2 \rangle$ (and $\langle q'^2 \rangle$) at various x . A fit of the x -dependence to the expected parabola yields a value for χ_t .

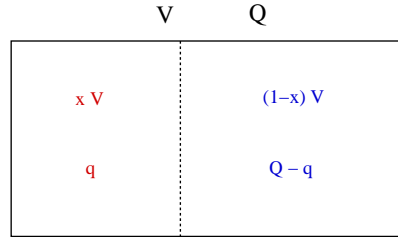


Figure 1: Division of a volume V into *slabs* of sizes xV and $(1-x)V$, with topological charges $q, Q-q \in \mathbb{R}$.

3. Results

3.1 Quantum rotor

We start with high-precision results for the quantum rotor (or 1d XY model, or 1d O(2) model) [14]. Each site of a periodic lattice in Euclidean time carries an angular variable ϕ_t , and we define the topological charge geometrically,

$$Q[\phi] = \frac{1}{2\pi} \sum_t \Delta\phi_t, \quad \Delta\phi_t = (\phi_{t+1} - \phi_t) \bmod 2\pi \in (-\pi, \pi]. \quad (3.1)$$

We consider three lattice actions,

$$S_{\text{standard}}[\phi] = \beta \sum_t (1 - \cos(\Delta\phi_t)), \quad S_{\text{Manton}}[\phi] = \frac{\beta}{2} \sum_t (\Delta\phi_t)^2, \quad S_{\text{constraint}}[\phi] = \begin{cases} 0 & |\Delta\phi_t| < \delta \quad \forall t \\ +\infty & \text{otherwise.} \end{cases}$$

Typical results for $\langle q^2 \rangle$ and $\langle q'^2 \rangle$ are shown in Fig. 2. In each case they match the expected parabola to high accuracy; this parabola connects $\langle q^2 \rangle|_{x=0} = 0$ with $\langle q^2 \rangle|_{x=1} = Q^2$, and $\langle q'^2 \rangle|_{x=0} = 0$ with $\langle q'^2 \rangle|_{x=1} = 0$; the latter is predicted as $L\chi_t x(1-x)$.

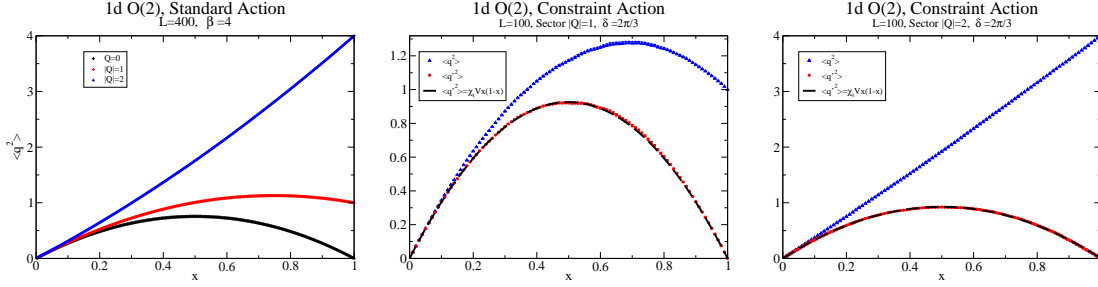


Figure 2: Left: $\langle q^2 \rangle$ measured for S_{standard} ($L = 400$, $\beta = 4$) in the sectors $|Q| = 0, 1, 2$. Centre/right: $\langle q^2 \rangle$ and $\langle q'^2 \rangle$ for $S_{\text{constraint}}$ ($L = 100$, $\delta = 2\pi/3$) at $|Q| = 1$ (centre) and $|Q| = 2$ (right).

Now we consider the results for the scaling quantity $\chi_t \xi$, where ξ is the correlation length. For all three lattice actions the value is known analytically [18, 19] in the thermodynamic limit, $L \rightarrow \infty$. The plots in Fig. 3 illustrate the convergence towards these values (horizontal lines) at fixed β , for increasing size. This convergence is manifest, but slow: in particular for the standard action there are permille level finite size effects even at $L/\xi > 30$; these effects are enhanced for increasing $|Q|$.

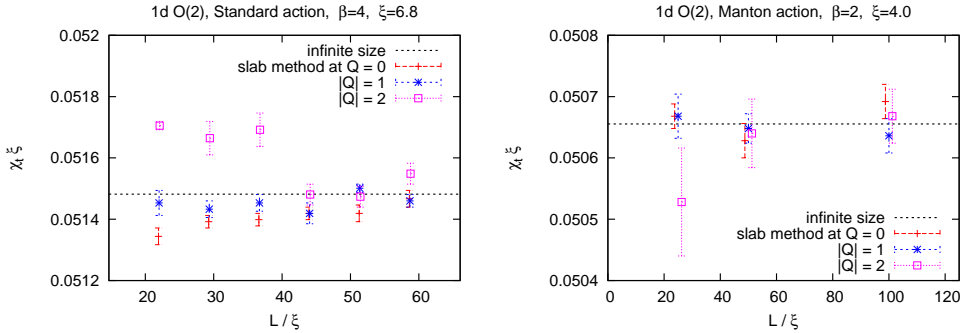


Figure 3: The finite size scaling of $\chi_t \xi$, for the standard action at $\beta = 4$, and for the Manton action at $\beta = 2$.

3.2 Heisenberg model

We proceed to the 2d Heisenberg model, or $O(3)$ model. Here the “scaling term”, $\chi_t \xi^2$, diverges logarithmically in the continuum limit, see *e.g.* Ref. [19]. Hence we consider just χ_t at finite ξ (in lattice units). Again we apply the geometric definition for Q [20], and we consider the three lattice actions, which are analogous to Subsection 3.1. Fig. 4 shows that the results are very close to the directly measured values of χ_t ; those are precise in this case, thanks to the use of the Wolff cluster algorithm, which avoids topological freezing. The data are given in Ref. [14].

We also consider the kurtosis c_4 ,

$$c_4 = \frac{1}{V} \left(3\langle Q^2 \rangle^2 - \langle Q^4 \rangle \right), \quad (3.2)$$

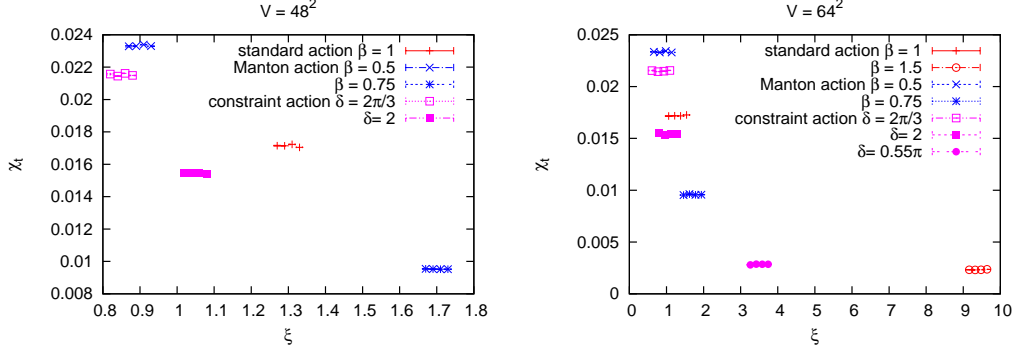


Figure 4: Data for the 2d $O(3)$ model in $V = 48^2$ and 64^2 : each quadruplet of points shows (from left to right) the directly measured χ_t , and the values obtained by the slab method in the sectors $|Q| = 0, 1, 2$.

which represents a measure of the deviation from a Gaussian distribution (where c_4 vanishes). Fig. 5 shows the convergence of the (dimensionless) ratio c_4/χ_t in the continuum limit towards $\simeq -1$, the value for a dilute instanton gas; this is best visible for the Manton action.² Comparing the two plots in Fig. 5 suggests that — in this regime — the volume hardly affects the ratio c_4/χ_t .³

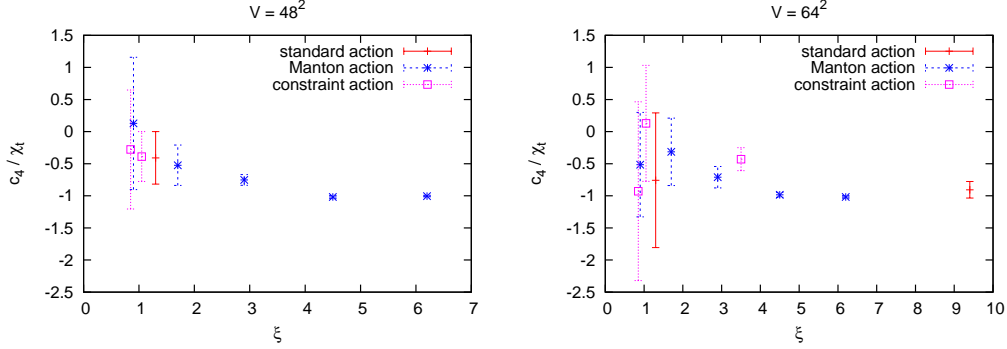


Figure 5: Dependence of c_4/χ_t on the correlation length ξ , for different lattice actions and volumes.

3.3 2-flavour QCD

Finally we proceed to 2-flavour QCD, formulated with the Wilson gauge action. The topological charge density is constructed from the standard lattice field strength tensor. After smoothing, $\sum_x q_x$ is slightly re-scaled (for optimal proximity to integers [4]) and then rounded to $Q \in \mathbb{Z}$.

For the quarks we used twisted mass fermions (full twist, bare mass 0.015), which leads to a somewhat heavy pion mass, $M_\pi \simeq 650 \text{ MeV}$ (here we are only interested in testing the slab method). The statistics involved 20000 configurations, in $V = 16^3 \times 32$ (and slab volumes $16^3 \times 32x$ and $16^3 \times 32(1-x)$) at $\beta = 3.9$, which implies a lattice spacing of $a \simeq 0.079 \text{ fm}$.

Smoothing was performed by the gradient flow (or Wilson flow in this case), with Runge-Kutta integration in the flow time t (step sizes 0.01 and 0.001 yield consistent results). The reference point proposed by Lüscher [22], $t_0^2 \langle E \rangle_{\text{plaquette}} = 0.3$, requires the flow time $t_0 = 2.42$.

Fig. 6 (left) shows data for $\langle q'^2 \rangle$ from $|Q| = 0, 1, 2$, after flow time $t = 5t_0$ [15]. At extreme values, $x \gtrsim 0$ and $x \lesssim 1$ (where thin slabs are involved), the data deviate from a parabolic shape.

²In $d = 1$ the Manton action is classically perfect [18], which explains its excellent scaling behaviour. Apparently its 2d version was used first in Ref. [14], and it has favourable properties as well.

³This quantity has been investigated extensively in 4d $SU(3)$ Yang-Mills theory, see *e.g.* Refs. [21]. According to the latest studies, c_4/χ_t converges of to a small but finite value around -0.26 in the continuum and infinite volume limit.

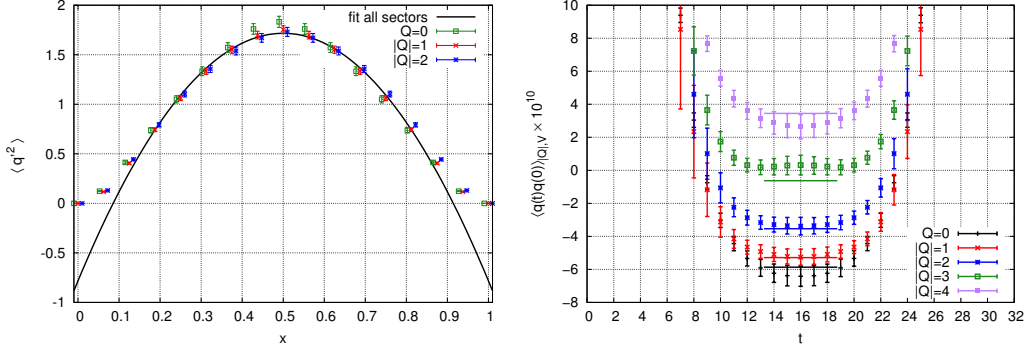


Figure 6: Left: $\langle q'^2 \rangle$ in 2-flavour QCD, after $t = 5t_0$, in $|Q| \leq 2$, and a global fit. Right: data and fits for the AFHO method [11], cf. eq. (1.3).

This effect, caused by smoothing, is exponential; at $x \gtrsim 0$ we observed: $|\text{deviation}| \propto \exp(-c(t)x)$. Therefore we focus on the interval $0.2 \leq x \leq 0.8$, and perform a joint fit — of all data for $|Q| \leq 2$ — to the shifted parabola

$$\langle q'^2 \rangle = V\chi_t x(1-x) + \text{const.}, \quad (3.3)$$

which is shown in Fig. 6. This fit works well, and it yields a result for χ_t , which perfectly agrees with a direct measurement, and with the result of the AFHO method [11] (cf. Section 1),

$$\chi_t a^4 = \begin{cases} 7.76(20) \cdot 10^{-5} & \text{direct} \\ 7.63(14) \cdot 10^{-5} & \text{slab method for } |Q| \leq 2 \\ 7.69(22) \cdot 10^{-5} & \text{AFHO method for } |Q| \leq 2. \end{cases} \quad (3.4)$$

Regarding the AFHO method, which refers to formula (1.3), the correlations of the topological charge density and the plateau values (after flow time $t = 6t_0$) are shown in Fig. 6 on the right.

Fig. 7 (left) illustrates the evolution of $\langle q'^2 \rangle$ for flow time $t_0 \dots 5t_0$, in the sector with $Q = |1|$ (as an example). Longer flow time reduces the statistical errors (the configurations are smoother), but the deviations at the extreme values of x are enhanced, and the additive constant in eq. (3.3) becomes more negative. This constant is required here, but it has not been anticipated in the

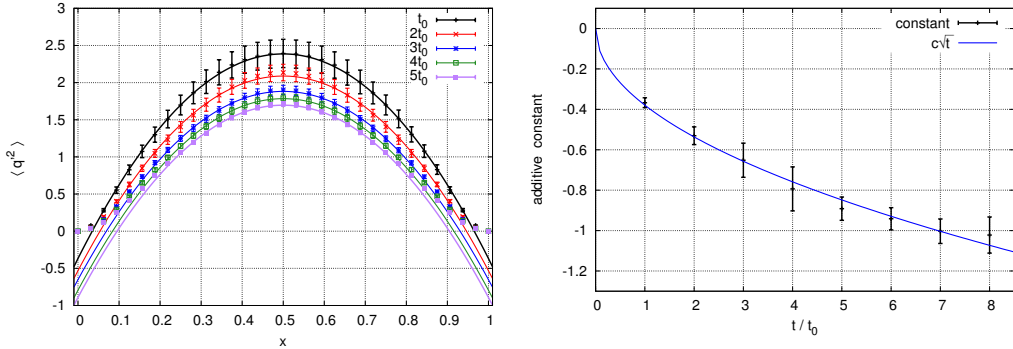


Figure 7: Left: $\langle q'^2 \rangle$ in 2-flavour QCD at $|Q| = 1$, at flow times $t = t_0 \dots 5t_0$. Even in the range $t = t_0 \dots 8t_0$, the value for $\chi_t a^4 \cdot 10^5$ — from a fit to eq. (3.3) — is stable within errors (e.g. $t_0 : 7.70(20)$, $2t_0 : 7.69(21)$, $4t_0 : 7.67(18)$, $6t_0 : 7.80(18)$, $8t_0 : 7.90(20)$). Right: the additive const. of eq. (3.3) as a function of t .

slab formula (2.1). The plot in Fig. 7 on the right shows that it is consistent with a behaviour $\text{const.} \propto \sqrt{t}$, which corresponds to a diffusion process. If we fit the data to the ansatz $c_1 \sqrt{t} + c_2$, we obtain $c_2 = 0.003(18)$, which confirms that this constant (practically) vanishes at $t = 0$.

4. Conclusions

The slab method is a simple and robust procedure to measure χ_t within a fixed topological sector. Hence it is not affected by “topological slowing down”, and it hardly costs any computing time, but there are persistent finite size effects (they tend to be polynomial at fixed topology [8–12, 14]). It works best at small $|Q|$, which is also the case for the alternative fixed topology methods of Refs. [8, 11]. In contrast to them, however, the *only* assumption needed for the slab method is a Gaussian distribution of the topological charges, which holds to a very good approximation.⁴

We reviewed successful tests in $O(N)$ models [14] and in 2-flavour QCD [15]. In the 2d $O(3)$ model we obtained correct results for χ_t to %-level, and in the 1d $O(2)$ model far beyond. In 2-flavour QCD, %-level precision is attained as well, after gradient flow times $t = t_0 \dots 8t_0$. Here an additive constant is required in the fit, and one has to exclude small intervals of x close to 0 and 1.

References

- [1] O. Wantz and E.P.S. Shellard, *Phys. Rev.* **D 82** (2010) 123508. C. Bonati *et al.*, *JHEP* **1603** (2016) 155. P. Petreczky, H.-P. Schadler and S. Sharma, arXiv:1606.03145 [hep-lat]. Sz. Borsanyi *et al.*, arXiv:1606.07494 [hep-lat]. V. Azcoiti, arXiv:1609.01230 [hep-lat].
- [2] W. Bietenholz and S. Shcheredin, *Nucl. Phys.* **B 754** (2006) 17.
- [3] A. Bazavov *et al.* (MILC Collaboration), *Rev. Mod. Phys.* **82** (2010) 1349.
- [4] L. Del Debbio, H. Panagopoulos and E. Vicari, *JHEP* **0208** (2002) 044.
- [5] S. Schaefer, R. Sommer and F. Virota (ALPHA Collaboration), *Nucl. Phys.* **B 845** (2011) 93.
- [6] M.G. Endres, these proceedings.
- [7] M. Lüscher and S. Schaefer, *JHEP* **1107** (2011) 036.
- [8] R. Brower, S. Chandrasekharan, J.W. Negele and U.-J. Wiese, *Phys. Lett.* **B 560** (2003) 64.
- [9] A. Dromard and M. Wagner, *Phys. Rev.* **D 90** (2014) 074505.
- [10] W. Bietenholz *et al.*, *Phys. Rev.* **D 93** (2016) 114516.
- [11] S. Aoki, H. Fukaya, S. Hashimoto and T. Onogi, *Phys. Rev.* **D 76** (2007) 054508.
- [12] I. Bautista *et al.*, *Phys. Rev.* **D 92** (2015) 114510.
- [13] P. de Forcrand *et al.*, *Nucl. Phys. (Proc. Suppl.)* **73** (1999) 578.
- [14] W. Bietenholz, P. de Forcrand and U. Gerber, *JHEP* **1512** (2015) 070.
- [15] A. Dromard, W. Bietenholz, K. Cichy and M. Wagner, *Acta Phys. Polon. Supp.* **9** (2016) 635.
- [16] R.C. Brower *et al.* (LSD Collaboration), *Phys. Rev.* **D 90** (2014) 014503.
- [17] E.V. Shuryak and J.J.M. Verbaarschot, *Phys. Rev.* **D 52** (1995) 295.
- [18] W. Bietenholz, R. Brower, S. Chandrasekharan and U.-J. Wiese, *Phys. Lett.* **B 407** (1997) 283.
- [19] W. Bietenholz, U. Gerber, M. Pepe and U.-J. Wiese, *JHEP* **12** (2010) 020.
- [20] B. Berg and M. Lüscher, *Nucl. Phys.* **B 190** (1981) 412.
- [21] S. Dürr *et al.*, *JHEP* **0704** (2007) 055. L. Giusti, S. Petrarca and B. Taglienti, *Phys. Rev.* **D 76** (2007) 094510. H. Panagopoulos and E. Vicari, *JHEP* **1111** (2011) 119. M. Cè *et al.*, *Phys. Rev.* **D 92** (2015) 074502. C. Bonati, M. D’Elia and A. Scapellato, *Phys. Rev.* **D 93** (2016) 025028.
- [22] M. Lüscher, *JHEP* **1008** (2010) 071; PoS(LATTICE2010) 015.

⁴A generalisation which incorporates higher moments in the Q -distribution is feasible as well.